FTIR Spectroscopy of Alcohol and Formate Interactions with Mesoporous TiO_2 Surfaces

Jeffrey R. S. Brownson,[‡] M. Isabel Tejedor-Tejedor,[§] and Marc A. Anderson*[,§]

CNRS Institut des Sciences Chimiques Seine-Amont, 2-8 rue Henri Dunant, 94320 THIAIS, France, and Environmental Chemistry and Technology Program, University of Wisconsin—Madison, 660 N. Park Street, Madison, Wisconsin, 53706

Received: March 9, 2006; In Final Form: May 2, 2006

The effects of pH and ultraviolet (UV) light with ligated formic acid on mesoporous TiO_2 were characterized by transmission Fourier transform infrared (FTIR) spectroscopy and compared with adsorbed formate complexes. Surface-modified anatase thin films were prepared from acidic aqueous nanoparticulate anatase suspensions diluted with methanol and ethanol. Bands assigned to carboxylic acid groups displayed unique bonding character in the ligated formic acid on the anatase surface. For increased proton concentrations in the films, separation in −COO stretching bands ($\Delta\nu$) for formic acid increased (increase in frequency for νC═O and decrease in frequency for νC−O). With UV exposure, surface-bound organics were rapidly removed by photocatalytic oxidation at 40 °C and 40% relative humidity (RH). In addition, the $\Delta\nu$ of the formic acid bands decreased as organics were mineralized to carbonates and CO_2 with UV light. Aqueous formic acid adsorption experiments showed a distinctly different bonding environment lacking carbonate, and the $\Delta\nu$ for the carboxylic groups indicated a bridging bidentate coordination. The $\Delta\nu$ of the bands increased with increasing proton concentration, with both bands shifting to higher wavenumbers. The shifts may be ascribed to the influence of protonation on surface charge and the effect of that charge on the electronegativity of carboxylate groups bound to the surface. As alcohols are used in the mesoporous TiO_2 solar cell preparation, implications of these surface modifications to dye-sensitized photovoltaics are discussed.

Introduction

The search for alternative energy sources has led to the development of dye-sensitized photovoltaics, or "Grätzel cells".[1] The two components that stand apart in importance are the nanocrystalline anatase xerogel film and the metal-organic dye that is impregnating the highly porous and tortuous film. The dyes are often bound to the anatase surface using carboxylic moieties as terminal sites, typically using a (2,2′-bipyridal-4,4′-dicarboxylate)Ru(II) structure.[2,3] A primary role of the mesoporous, semiconducting TiO_2 ceramic is to establish an extremely high surface area within a thin film, generating a surface-enhanced signal for interfacial molecules per unit mass oxide in comparison to single crystals or large particles. In the case of TiO_2 photovoltaics, the effect is translated into a surface area-dependent photocurrent. This is crucial, as the functional portion of the light-absorbing dye is the monolayer in direct contact with the titania surface.[4] It has already been demonstrated that the proton character of the anatase film surface can affect the electron-shuttling properties of the light-absorbing dye to a titania interface. Higher proton concentrations promote rapid oxidation−reduction reactions in the surficial dyes and increase electron injection yields and hence are desirable in a prepared film.[5]

Preparation techniques in titania film processing often use alcohols for depositing uniform films[6] or as solvents to assist in impregnating the dyes within the film.[2] For highly protonated surfaces, the alcohol has been found to react with the surface hydroxides of anatase via a reesterification reaction, creating a layer of surface alkoxides.[7] As we have reported previously, the alkoxide is rapidly oxidized to organic surface species that have distinctly different bonding characters from those measured by aqueous adsorption experiments of organic acids such as formic acid.[8] In this paper, we have continued to characterize the ligated formic acid species via Fourier transform infrared (FTIR) spectroscopy. In so doing, we have studied the shifts in IR band positions for the carbonyl/carboxylate species and oxidation products with respect to changes in proton concentration and UV exposure. Given the prevalence of alcohol use in thin-film preparation processes, we also discuss the effect of short chain alcohol adsorption on films prepared in this fashion.

Experimental Methods

Nanoparticulate suspensions of anatase phase TiO_2 (sols) used in this study were synthesized as described previously.[7,8] Briefly, titania sols were adjusted to three initial values of pH (1.4, 2.3, 3.1) and each diluted with ethanol or methanol (8 g/L total solid content) to achieve mole fractions of alcohol $X_{ROH} = 0.33$, 0.40, and 0.48 for comparison. To maintain the solids concentration for each alcohol, a balancing mole fraction of water of the desired pH was added. Inorganic films prepared without diluting with alcohol ($X_{ROH} = 0$) at pH 3.1 were also prepared and tested for aqueous formic acid adsorption. The inorganic films were dried under vacuum and then dipped into a 0.05 M formic acid solution that was adjusted to one of three values of pH (1.4, 2.3, 3.1). The films were soaked for 2 h and then dried and characterized by FTIR spectroscopy. Results were compared to the data sets for MeOH and EtOH dilutions.

Coating was performed using a low-pressure ultrasonic spray system, also described previously.[7,8] The system delivered

* To whom correspondence should be addressed. E-mail: nanopor@wisc.edu. Tel: 1 608 262 2674. Fax: 1 608 262 0454.
‡ CNRS Institut des Sciences Chimiques Seine-Amont.
§ University of Wisconsin.

10.1021/jp0614547 CCC: $33.50
Published on Web 06/03/2006

uniform coatings on the Si wafers that gelled quickly, with thicknesses between 150 and 300 nm. All films were dried and stored under vacuum immediately after deposition to minimize hydrolysis reactions of the surface organics. These films were all used within 2 days of coating.

All UV exposures used 254 nm light from a 500 W Oriel Xe(Hg) arc lamp as described in our earlier studies.[7,8] This wavelength is the peak irradiance of a UVB germicidal Hg fluorescent bulb, a readily available light source. A Czerny-Turner monochromator with 3 mm slit widths was used to select a chosen wavelength. A sealed, UV opaque poly(methyl methacrylate) (PMMA) box was created for a controlled environment of exposure (28.32 L/1 ft^3). The reactor was humidified to 40% relative humidity (RH) at 40 °C. Internal silicone-coated heat tape and a 2.5 W fan created a well-mixed environment within the reactor. The box was fitted with a 50 mm fused silica window (UV transparent) to allow the high-energy light to pass. For all experiments, a 20 J cm^{-2} fluence was employed in the photoreaction.

FTIR data were collected with a Nicolet Magna 750 spectrometer in transmission mode as described previously (4000−900 cm^{-1}, 150 scans, 1 cm^{-1} resolution).[7,8] Si wafers were used as IR-transparent substrates. All Si wafers were placed inside a cell with BaF_2 windows and flushed with zero-air for initial background collection. Following the spray deposition of the TiO_2 sol and vacuum-drying, the films were immediately transferred to the IR cell and flushed with zero-air for 1 h 30 min. Dry spectra were then collected for films prior to UV exposure. The wafers were subsequently transferred into the UV reactor for a 20 J cm^{-2} exposure and then carefully replaced in the IR cell for a final post-UV spectral collection. All spectra were processed for interferometric noise reduction, background subtraction, and peak deconvolution using RazorTools/8 Bayesian data analysis programs via the Grams/AI software package. Spectra from 1800 to 1050 cm^{-1} were normalized to a consistent sharp band at 1582 cm^{-1} (assigned to a bidentate carbonate νCO_{II} stretching mode) unless mentioned otherwise in the figures.[8−13] This band changed minimally in all photocatalytic oxidation experiments. By normalizing to this band we could compensate for slight differences in film thickness due to viscosity variations between methanol- and ethanol-diluted sols.

Results

The full IR spectra of these systems have been presented previously.[8] Therefore, here we focus our discussion on the specific bands of interest. Figure 1 presents a comparison of alkoxide and hydroxide bands at the surface, displaying that for dark dry conditions and lower proton concentrations the bands for alkoxide C−O stretching modes and alkoxide methyl/methylene stretching modes are present in the spectra of both methanol and ethanol systems. This confirms that the reesterification process is occurring for both dilutions. The intensity of the alkoxide bands is reduced by increasing the proton concentration in the film and with the addition of humidity. The methanol spectra in Figure 1A displays a methoxide band at 1137 cm^{-1}. This is in close agreement with previous studies of methoxide formation by esterification from adsorbed methanol.[8,14,15] Corresponding methyl stretching modes were assigned to bands at 2928 and 2831 cm^{-1}. These were assigned to the asymmetric and symmetric methyl stretching modes of surface methoxy species. These IR bands have been reported in other studies and similarly assigned.[8,14,15]

The spectra of the ethanol system for pH 3.1 in Figure 1B displayed bands at 1129 and 1074 cm^{-1}. These were assigned

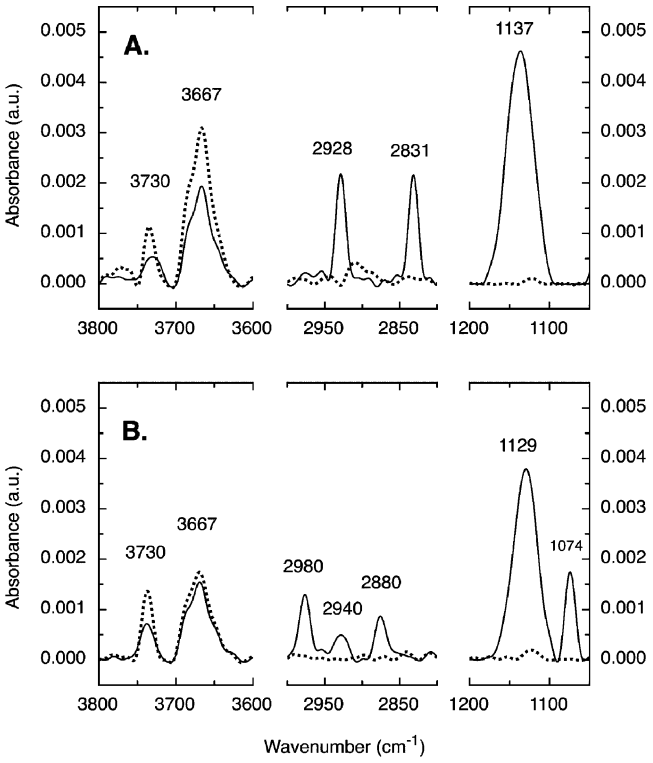

Figure 1. Segmented IR spectra from 3800 to 1050 cm^{-1} for films prior to UV exposure (solid line) and following 20 J cm^{-2} UV exposure (dashed line): (A) methanol-diluted films from pH 3.1 sols and (B) ethanol-diluted films from pH 3.1 sols.

to the νC−O and νC−C modes of the ethoxy surface species, respectively.[8,17] The alkoxide peaks were consistent with spectra found by other investigations regarding ethanol esterification to ethoxide on anatase surfaces.[7,8,14] Again, corresponding peaks at 2980, 2940, and 2880 cm^{-1} were assigned to the characteristic symmetric and asymmetric stretching modes of $-CH_2-$ and $-CH_3$ species in the surface alkoxide. Following UV exposure, under humid environmental conditions, the alkoxide bands were absent. Removal of these bands coincided with the complete removal of methylene and methyl stretching bands. Also in Figure 1, the spectra for both alcohol systems display two distinct bands at 3730 and 3667 cm^{-1}, which were previously assigned to stretching modes of non-hydrogen bonded anatase surface −OH groups.[8] These bands showed a small increase in absorption intensity following UV exposure.

Figure 2 shows the diagnostic region for the carboxylic functional groups in the spectra of both MeOH and EtOH derived films prior to UV exposure (1750 to 1150 cm^{-1}, pH 1.4, $X_{ROH} = 0.48$). This figure also illustrates the deconvolved spectra of these films. One can see a striking similarity in the profile of the spectra for films from different parent conditions. Peaks in this region, the most intense in the spectra associated with the organic species, were present immediately after drying the films (Figure 3A). Their intensity was found to be proportional to the proton concentration in the films.[8] According to previous results, bands at ∼1605 and ∼1295 cm^{-1} should be assigned to the νC═O and νC−O modes of a molecular formic acid bound to the surface as a highly asymmetric ligated structure.[8] As can be seen in Table 1, the wavenumber separation (termed $\Delta\nu$) for the carboxylate bands increased with increasing proton concentration in the films prior to UV exposure. Specifically, the band assigned to νC═O shifted to higher wavenumbers, while the band assigned to νC−O shifted to lower wavenumbers. Following UV irradiation, the change in $\Delta\nu$ was

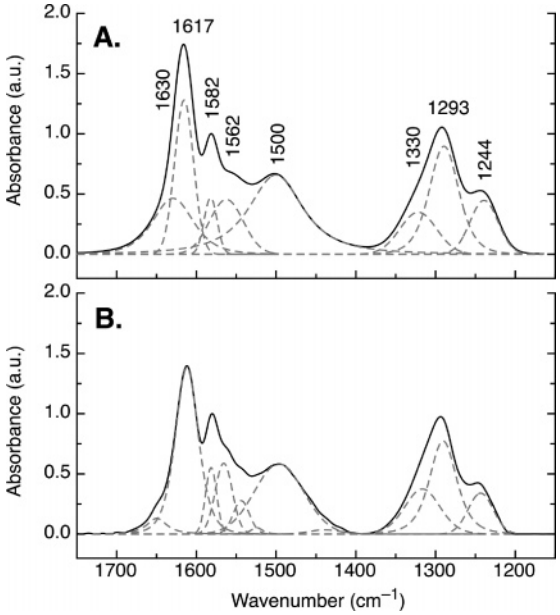

Figure 2. Deconvolved IR spectra from 1750 to 1150 cm^{-1} for films prior to UV exposure: (A) pH 1.4 methanol diluted films and (B) pH 1.4 ethanol diluted films.

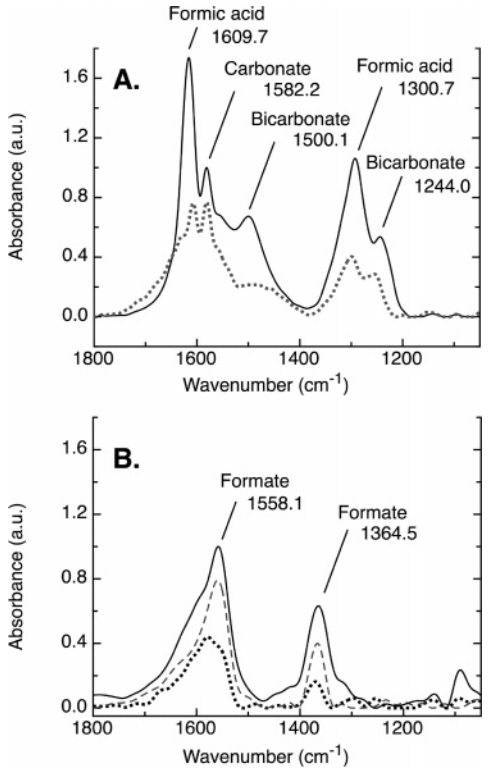

Figure 3. (A) pH 1.4 methanol-diluted spectra for films prior to UV exposure (solid line) and following 20 J cm^{-2} UV exposure (dashed line). Spectra were normalized to the carbonate band at 1582 cm^{-1} and labeled according to the pH of inital sol. (B) IR spectra of inorganic anatase film dipped into 0.05 M formate solutions adjusted to pH 3.1 (solid), 2.3 (dashed gray), and 1.4 (dotted). Spectra were normalized to the maximum intensity peak for pH 3.1 film.

found to decrease, again in proportion to proton concentration. This is represented in Table 2 as $\Delta\Delta\nu$. The large $\Delta\Delta\nu$ found for high proton concentrations was observed as a decrease in wavenumber for νC═O and an increase in wavenumber for the νC−O band. By comparing the peak positions between methanol and ethanol, we see that the alcohol used in synthesis did not significantly affect the position of these bands.

TABLE 1: Positions of Carboxylic Stretching Frequencies for Formic Acid Prior to UV Exposure (Alcohol System)

	pH	νC═O	νC−O	$\Delta\nu$
Methanol	1.4	1616.7	1292.5	324.2
	2.3	1608.8	1296.1	312.7
	3.1	1605.5	1295.6	309.9
Proton Shift (cm^{-1})		*−11.2*	*+3.1*	*−14.3*
Ethanol	1.4	1616.7	1294.6	322.1
	2.3	1609.7	1296.7	313.0
	3.1	1604.5	1300.6	303.9
Proton Shift (cm^{-1})		*−12.2*	*+6.0*	*−18.2*

TABLE 2: Positions of Carboxylic Stretching Frequencies For Formic Acid Following UV Exposure (Alcohol System)

	pH	νC═O	νC−O	$\Delta\nu$	$\Delta\Delta\nu$
Methanol	1.4	1609.7	1300.7	309.0	−15.2
	2.3	1605.4	1301.1	304.3	−8.4
	3.1	1605.7	1297.3	308.4	−1.5
Proton Shift (cm^{-1})		*−4.0*	*−3.4*	*−0.6*	
Ethanol	1.4	1606.5	1299.9	306.6	−15.5
	2.3	1605.3	1297.6	307.7	−5.3
	3.1	1606.5	1299.2	307.3	3.4
Proton Shift (cm^{-1})		*+0.0*	*−0.7*	*+0.7*	

In Figure 2A, a shoulder near 1630 cm^{-1} was assigned to the bending mode of pore water in the film. Bands at ∼1582 and ∼1330 cm^{-1}, along with a weak band at ∼1010 cm^{-1} in the broader spectra, were assigned to νCO_{II}, $\nu CO_I + \delta O_I CO_{II}$, and νCO_I modes of a bidentate carbonate (CO_2^{-3}) surface species, respectively.[9−13] These bands were in agreement with studies reporting bidentate carbonate surface formation on anatase.[9−13] The bands did not shift significantly with changes in pH or UV exposure (see νCO_{II} in Table 3). Also in Figure 2A and Table 3, bands at ∼1562, a broad band between ∼1500 and 1480, and at ∼1245 cm^{-1} were each assigned to the ν_aCO, ν_sCO, and δOH···O modes of a bidentate bicarbonate (HCO_3^-) species, respectively.[10,11] The strong band assigned to ν_sCO shifted up in wavenumber with increased proton concentration, while the band assigned to δOH···O decreased in wavenumber. In each of the alcohol-diluted films, the bands associated with the formic acid and HCO_3^- species showed an increase in intensity with increasing proton concentration. There was a corresponding decrease in intensity of those peaks relative to those belonging to the CO_3^{-2} species following UV exposure.

We show in Figure 3B the bands associated with adsorbed formic species produced by treating the TiO_2 with an aqueous solution of formic acid. These bands were assigned to ν_aCOO and ν_sCOO modes of a bridging bidentate formate complex.[8] The values for the $\Delta\nu$ between these bands (<208 cm^{-1}) for different solution conditions, reported in Table 4, were much smaller than those observed for the surface bound formic species in alcohol systems. In the water systems, the higher frequency band is observed at lower frequencies compared to the alcohol-modified systems (1558.1 vs 1605 cm^{-1}) and the lower frequency band at higher frequencies (1364.5 vs 1295 cm^{-1}). These contrasting spectra suggest the formation of more asymmetric surface bound formate/formic species in the alcohol-modified systems, as in the model proposed above. Additionally, it was found that, in the water systems, both of the carboxylate bands increased in frequency with increasing proton concentration, with a net increase in $\Delta\nu$. There was no evidence of peaks associated with bicarbonate or carbonate complexes in these spectra.

TABLE 3: Positions of Carbonate and Bicarbonate Peaks in Alcohol Systems with Respect To Proton Concentration (Excluding Deconvolved Bands)

		prior to UV exposure			following UV exposure		
	pH	νCO_{II} carbonate	$\nu_a CO$ bicarbonate	$\nu OH\cdots O$ bicarbonate	νCO_{II} carbonate	$\nu_a CO$ bicarbonate	$\nu OH\cdots O$ bicarbonate
Methanol	1.4	1582.2	1500.1	1244.0	1582.1	1482.4	1250.6
	2.3	1583.7	1490.1	1248.6	1582.7	1483.6	1251.7
	3.1	1582.4	1483.6	1251.5	1582.5	1485.8	1250.1
Proton Shift (cm^{-1})		*−0.2*	*+16.5*	*−7.5*	*−0.4*	*−3.4*	*+0.5*
Ethanol	1.4	1582.6	1495.5	1247.4	1581.7	1479.4	1250.9
	2.3	1583.6	1489.1	1249.3	1582.5	1473.5	1251.3
	3.1	1581.3	1481.4	1256.1	1583.0	1482.2	1253.1
Proton Shift (cm^{-1})		*+1.3*	*+14.1*	*−8.7*	*−1.3*	*−2.8*	*−2.2*

TABLE 4: Positions of Carboxylic Stretching Frequencies For Aqueous-Adsorbed Formate

	pH	$\nu_a COO$	$\nu_s COO$	$\Delta\nu$
Water (HNO_3)	1.4	1578.4	1370.3	208.1
	2.3	1559.1	1366.3	192.8
	3.1	1558.1	1364.5	193.6
Proton Shift (cm^{-1})		*+20.3*	*+5.8*	*−14.3*
Ionic Formate[a]		1567	1366	201

[a] Free ionic formate data from literature for comparison (ref 17).

Discussion

The wavenumber separation of the −COO stretching bands is a good diagnostic of the binding environment for the carboxylate species, relative to the aqueous ionic species, in the case of formate $\Delta\nu = 201$ cm^{-1} (see Table 4). For example, monodentate complexes display $\Delta\nu$ values much larger than ionic complexes, bidentate/chelating complexes exhibit values much less than ionic complexes, and bridging bidentate complexes display values larger than chelating complexes but near the ionic value.[13] However, it is apparent that as one alters the proton concentration in the film, there are more data than the $\Delta\nu$ alone to provide insight in this investigation. Hence, the changes in both the band position and the separation of bands assigned to the −COO species have been considered.

The frequencies of the stretching modes reflect the carbon acidity and the bond strength of the complexed carboxylate/carboxylic acid. The acidity of the carboxylic moiety (as R−COOH) depends on the electron density of surrounding moieties, such as the R group or neighboring surface species. For an electron-withdrawing species, the carboxylic carbon will be more electropositive, increasing the density between the carbon−oxygen bonds. This results in an increase of both νC═O and νC−O band frequencies. Conversely, for a species that is more electron-donating, both bands will appear at lower frequencies. Of course, for formic acid the R group modifying the carboxylic carbon is hydrogen, but the surface environment of photoactivated anatase can be populated by a large quantity of electron-rich peroxide or superoxide surface species generated during photocatalytic oxidation. The carboxylic carbon may form weak bonds with these species such that the H−C bond does not break. This would increase the electron density of the carboxylic carbon atom, decreasing the frequencies for the −COO vibrations as seen in the $\Delta\Delta\nu$ results of Table 2. This type of complex could also be interpreted as a precursor for the formation of carbonate species at the surface.

We have previously proposed that ligated formic acid has an asymmetry such that the carbon−oxygen stretching modes do not couple with each other, thus the modes in ligated formic (termed νC═O and νC−OH) are independent.[8] The higher frequency band in the ligated formic acid is observed at a higher wavenumber than that of the bidentate ν_aCOO. However, the carbonyl group in free formic acid is observed at higher frequencies than in the ligated formic of our spectra, normally ∼1700 to 1680 cm^{-1}.[17] In fact, the higher frequency band appears at frequency values reported in the literature for monodentate formates (1604−1630 cm^{-1}).[13] Also, the lower frequency band of the ligated carboxylate associated with νC−O was observed at unusually low wavenumbers in comparison to the other monodentate bands in the literature (1315−1380 cm^{-1}).[13] The position of the two carboxylate bands can be explained by a surface complex in which the still protonated formic acid binds to a Ti ion through the carbonyl group, and the hydroxyl is hydrogen-bonded to a nearby surface oxygen. This molecular adsorption of formic acid has already been described in the literature as the most energetically favorable monodentate configuration.[18]

As seen in Table 1, there was a net decrease in $\Delta\nu$ as the proton concentration in the films was increased. However, upon further examination we show that the two carboxylic bands shifted in frequencies opposite to one another to adjust to the surrounding environment. In comparison with the formate adsorption results from the water system shown in Table 4, there was a similar decrease in $\Delta\nu$ with increasing proton concentration. In contrast to the alcohol-modified system, both bands shifted up in frequency with increasing proton concentration. The independent shifts for both bands of the alcohol-modified systems were interpreted as another indication of the decoupled band structure observed for the ligated formic acid species.

Similar shifts in frequency were found for the proposed bicarbonate modes displayed in Table 3. However, the distinct carbonate band (∼1582 cm^{-1}) did not shift with changes in proton concentration. The difference in behavior for the two species was interpreted as being due to the protonated state of the bicarbonate species versus the deprotonated state of the carbonate species.

As can be seen in Tables 1−3, all of the major bands between 1800 and 900 cm^{-1} tend to show minimal shifts in wavenumber following UV irradiation. Given the shifts prior to UV exposure of the proton-responsive bands, we propose that—in the process of completely mineralizing surface alkoxides to CO_2 gas—the concentration of available surface protons is reduced.

The experimental evidence for anatase-phase titania has demonstrated that the adsorption of small chain alcohols is a favorable interaction.[8,14−16] This has been confirmed using molecular-scale modeling of methanol.[16,18] However, interesting conclusions can also be acquired for a broader range of solvents by applying the continuum approximation of Landau and Liftshitz for weak interaction forces based on dielectric data as well. As pure water and alcohol solvents are nonionic, the Coulombic attractions have been assumed negligible as we investigate the weaker interaction forces involved. We show in

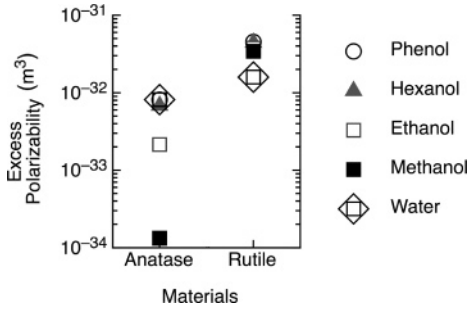

Figure 4. Calculated excess polarizabilities (absolute values) for solvent/mineral interactions. Values for neat molecules in their own continuum are on the order of $\sim(2-4) \times 10^{39}$ C^2 m^2 J^{-1}.

the Supporting Information that the reported values for permanent dipole moments of water and several short chain alcohols are quite similar, as are the total polarizabilities for both molecules.[19−21] Given the physical similarities of alcohol and water as solvating molecules, we must also consider the substrate. A solvent with a dielectric constant ϵ will be polarized by an applied field (E) and acquire an excess dipole moment. This will then affect the polarizability of the solvent, termed the excess polarizability. Assuming that mesoporous anatase acts as a surrounding medium of dielectric constant $\epsilon_{anatase}$, it will exert its own field, influencing the polarizabilities of the adsorbed solvent molecules. Hence, the surface molecules of a solid will reflexively alter the dielectric properties of the solvent by inducing an excess polarizability (α_i) on the solvating molecules as seen in the following equation:[19]

$$\alpha_i = 4\pi\epsilon_0\epsilon_f\left(\frac{\epsilon_i - \epsilon_f}{\epsilon_i + 2\epsilon_f}\right)a_i^3 = 3\epsilon_0\epsilon_f\left(\frac{\epsilon_i - \epsilon_f}{\epsilon_i + 2\epsilon_f}\right)v_i \qquad (1)$$

where a_i and v_i are the radius and volume of the solvent molecule, ϵ_i is the dielectric constant of the solvent molecule, and ϵ_f is the dielectric constant of a film of either anatase or rutile. In the case of a combination of molecules interacting with the surface, the molecule with the minimum excess polarizability is the one most similar to the adsorbed substrate. This minimum excess polarizability will be favored for preferentially interacting with the surface (essentially a case of "like attracts like"). We show our results in Figure 4. For anatase, the more favorable molecules for interactions are the short chain alcohols, preferentially methanol. In contrast, water is the preferred molecule for rutile surfaces. Hence, using the dielectric constants for anatase and rutile, we can see anatase is an interesting material for interactions with various solvents.

To summarize, we view this process of ligand formation as occurring in three stages. First, the alcohol needs to displace the water molecules and adsorb to the anatase surface. In displacing water molecules, the surface is effectively dried. Next, the alcohol needs a proton-rich environment to favor reesterification of the surface hydroxyls to form alkoxide functional groups. And finally, oxidation of the surface organics as proposed by the general reaction mechanism in Figure 5 needs to be accelerated by photocatalysis.

Conclusions

We have shown a major difference between the type of complexes of formic acid formed directly on an anatase surface due to photocatalytic oxidation and that formed by the adsorption of formic acid from aqueous solution. Both systems were established at pH well below the pK_a of proton dissociation for formic acid (pK_a = 3.75). Two types of bonding have been predicted by Vittadini et al. (a density-functional theory study using a generalized gradient approximation and a periodic slab geometry of the stoichiometric (101) anatase surface): a bridging bidentate conformation favored under hydrated conditions and a molecular monodentate formic acid species coordinated to a Ti through the carbonyl group and hydrogen bonded to a surface oxygen through the hydroxyl group favored for dry surface conditions.[18] We have already proposed that the ligated formic acid is generated as a result of photocatalytic oxidation of surface alkoxides also covalently bound, effectively establishing a "dry" anatase surface.[8] When formic acid interacts with a hydrated surface it tends to deprotonate and form bridging bidentate surface complexes. However, deprotonation on the dry surface of anatase seems to be more difficult, so the acid adsorbs in a molecular form. Hence, it is not unexpected to discover different binding conformations under varied conditions.

This study has important implications in the preparation of dye-sensitized photovoltaic cells. We have found that if small

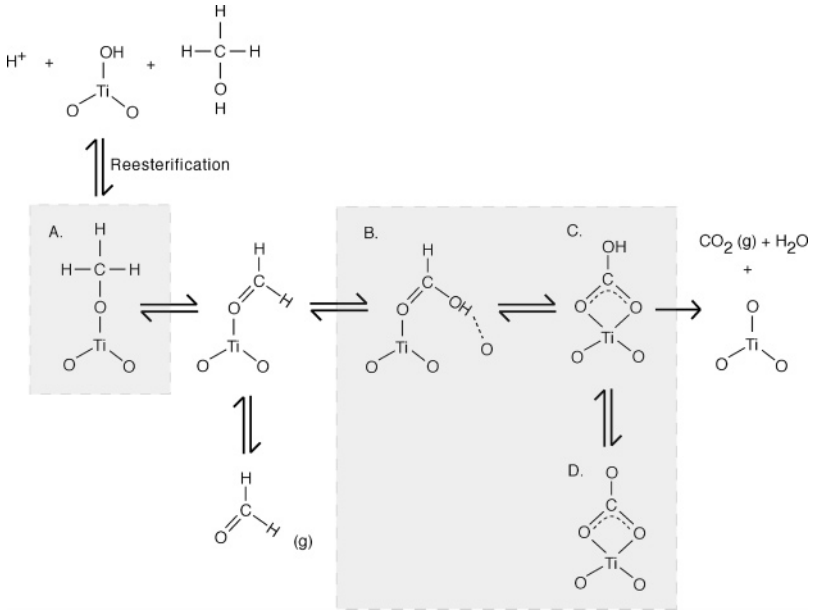

Figure 5. Proposed general mechanism for conversion of methanol to CO_2 and water. Grey boxes indicate surface species characterized by IR.

chain alcohols are used in the film preparation procedure, surface organics can form strong bonds with the anatase surface. Given that alcohols have been introduced in film preparation as a washing/cleansing step or as an added solvent to inject dyes into the pore structure[2,6] and given that dye-sensitized cells have been found to operate at higher photoefficiencies with higher proton concentrations in the film,[5] the presence of remnant surface organics is a valid issue. These bound ligands ultimately could be competing for adsorption sites with the dye ligands, modifying the electron-transfer efficiency within the dye-sensitized cells.

Acknowledgment. The authors sincerely thank Cardinal CG Co. (Eden Prairie, MN) for their financial support and enthusiastic discussions regarding this research.

Supporting Information Available: A table of dipole moments, total polarizabilities, dielectric constants, and calculated excess polarizabilities for water and various alcohol solvents in close proximity to anatase or rutile surfaces using the continuum approximation. This material is available free of charge via the Internet at http://pubs.acs.org.

References and Notes

(1) O′Regan, B.; Grätzel, M. *Nature* **1991**, *353*, 737.
(2) Nazeeruddin, M. K.; Kay, A.; Rodicio, I.; Humphrey-Baker, R.; Müller, E.; Liska, P.; Vlachopoulos, N.; Grätzel, M. *J. Am. Chem. Soc.* **1993**, *115*, 6382.
(3) McEvoy, A. J.; Grätzel, M. *Sol. Energy Mater. Sol. Cells* **1994**, *32*, 221.
(4) Gregg, B. A.; Pichot, F.; Ferrere, S.; Fields, C. L. *J. Phys. Chem. B* **2001**, *105*, 1422.
(5) Qu, P.; Meyer, G. J. *Langmuir* **2001**, *17*, 6720.
(6) Hagfeldt, A.; Boschloo, G.; Lindström, H.; Figgemeier, E.; Holmberg, A.; Aranyos, V.; Magnusson, E.; Malmqvist, L. *Coord. Chem. Rev.* **2004**, *248*, 1501.
(7) Brownson, J. R. S.; Lee, T. J.; Anderson, M. A. *Chem. Mater.* **2005**, *17* (11), 3025.
(8) Brownson, J. R. S.; Tejedor-Tejedor, M. I.; Anderson, M. A. *Chem. Mater.* **2005**, *17* (25), 6304.
(9) Yates, D. J. C. *J. Phys. Chem.* **1961**, *65*, 746.
(10) Morterra, C.; Chiorino, A.; Boccuzzi, F. *Z. Physik. Chem.* **1981**, *124*, 211.
(11) Busca, G.; Lorenzelli, V. *Mater. Chem.* **1982**, *7*, 89.
(12) Liao, L.-F.; Lien, C.-F.; Shieh, D.-L.; Chen, M.-T.; Lin, J.-L. *J. Phys. Chem. B* **2002**, *106*, 11240.
(13) Nakamoto, K. *Infrared and Raman Spectra of Inorganic and Coordination Compounds*, 5th ed.; John Wiley & Sons: New York, Vol. B, 1997.
(14) Burgos, M.; Langlet, M. *Thin Solid Films* **1999**, *349*, 19.
(15) Wu, W.; Chuang, C.; Lin, J. *J. Phys. Chem. B* **2000**, *104*, 8719.
(16) Wang, C.-Y.; Groenzin, H.; Schultz, M. J. *J. Phys. Chem. B* **2004**, *108*, 265.
(17) Roeges, N. P. G. *A Guide to the Complete Interpretation of Infrared Spectra of Organic Structures;* John Wiley & Sons: New York, 1994.
(18) Vittadini, A.; Selloni, A.; Rotzinger, F. P.; Grätzel, M. *J. Phys. Chem. B* **2000**, *104*, 1300.
(19) Israelachvili, J. N. *Intermolecular and Surface Forces*, 2nd ed.; Academic Press: San Diego, CA, 1992.
(20) Gonzalez, R. J.; Zallen, R.; Berger, H. *Phys. Rev. B: Condens. Matter Mater. Phys.* **1997**, *55* (11), 7014.
(21) Parker, R. A. *Phys. Rev. B: Condens. Matter Mater. Phys.* **1961**, *124* (6), 1719.